Science Bulletin 66 (2021) 257–264

Contents lists available at ScienceDirect

Science Bulletin

journal homepage: www.elsevier.com/locate/scib

Article

Conversion of bimetallic MOF to Ru-doped Cu electrocatalysts for efficient hydrogen evolution in alkaline media

Mengya Yang [a,1], Long Jiao [b,1], Huilong Dong [c,1], Liujiang Zhou [d,*], Changqing Teng [a], Dongming Yan [e], Tian-Nan Ye [f], Xiaoxin Chen [g], Yi Liu [a,*], Hai-Long Jiang [b,*]

[a] Institute for Composites Science Innovation (InCSI), School of Materials Science and Engineering, Zhejiang University, Hangzhou 310027, China
[b] Hefei National Laboratory for Physical Sciences at the Microscale, Department of Chemistry, University of Science and Technology of China, Hefei 230026, China
[c] School of Chemistry and Materials Engineering, Changshu Institute of Technology, Changshu 215500, China
[d] Institute of Fundamental and Frontier Sciences, University of Electronic Science and Technology of China, Chengdu 610054, China
[e] School of Civil and Architectural Engineering, Zhejiang University, Hangzhou 310058, China
[f] Materials Research Center for Element Strategy, Tokyo Institute of Technology, Yokohama 226-8503, Japan
[g] Center of Electron Microscopy and School of Material Science and Engineering, Zhejiang University, Hangzhou 310027, China

ARTICLE INFO

Article history:
Received 10 April 2020
Received in revised form 28 May 2020
Accepted 22 June 2020
Available online 26 June 2020

Keywords:
Metal–organic framework
Ru-doped Cu nanoparticles
Hydrogen evolution reaction
Alkaline media
Hydrogen adsorption energy

ABSTRACT

The rational design and construction of inexpensive and highly active electrocatalysts for hydrogen evolution reaction (HER) is of great importance for water splitting. Herein, we develop a facile approach for preparation of porous carbon-confined Ru-doped Cu nanoparticles (denoted as Ru-Cu@C) by direct pyrolysis of the Ru-exchanged Cu-BTC metal–organic framework. When served as the electrocatalyst for HER, strikingly, the obtained Ru-Cu@C catalyst exhibits an ultralow overpotential (only 20 mV at 10 mA cm^{-2}) with a small Tafel slope of 37 mV dec^{-1} in alkaline electrolyte. The excellent performance is comparable or even superior to that of commercial Pt/C catalyst. Density functional theory (DFT) calculations confirm that introducing Ru atoms into Cu nanocrystals can significantly alter the desorption of H_2 to achieve a close-to-zero hydrogen adsorption energy and thereby boost the HER process. This strategy gives a fresh impetus to explore low-cost and high-performance catalysts for HER in alkaline media.

1. Introduction

Hydrogen has been intensely investigated as an ideal energy carrier for sustainable energy economy due to its high energy density and environmentally friendly nature [1]. In spite of its paramount importance, the current industrial technologies for hydrogen production always rely on fossil fuels consumption, which will produce large amounts of CO_2 and increase greenhouse gases emissions [2]. In view of this, a more sustainable and eco-friendly strategy is urgently needed. Currently, the electrochemical hydrogen production by water splitting has been regarded as a promising technology for clean hydrogen production with a high efficiency [3]. As one of the key elements toward electrochemical hydrogen production, the highly active and extensively durable electrocatalysts are highly desired [4]. Generally, the reaction rate of hydrogen evolution reaction (HER) in acidic solution is much higher than that in alkaline solution. However, the extensive commercialization of water splitting in acidic media is severely limited by the scarcity of highly active and stable electrocatalysts to catalyze the oxygen evolution reaction (OER) at the counter electrode of HER [5]. Considering that the OER is more feasible in alkaline solution, it makes more sense to study HER in alkaline media. Compared with the direct H^+ reduction in acids, HER in alkaline media poses a significant challenge due to additional energy barrier from the extra water dissociation step, where the highly efficient electrocatalysts are highly desired [6].

It is well known that Pt-based nanocomposites are still the most efficient electrocatalysts for HER in alkaline media [7]. However, the high price and low abundance of Pt largely impede the large-scale commercial applications. Therefore, it is extremely desirable to design low-cost catalysts with high efficiency to replace Pt. In order to further reduce the price, minimizing noble metal loadings and utilizing noble-metal-free catalysts are two promising solutions to substitute Pt-based catalysts. Recently, the first-row transition-metal-based materials, as versatile noble-metal-free catalysts, have also attracted much attention for HER electrocatalysis [8,9]. Although the noble-metal-free electrocatalysts have

* Corresponding authors.
E-mail addresses: liujiang86@gmail.com (L. Zhou), liuyimse@zju.edu.cn (Y. Liu), jianglab@ustc.edu.cn (H.-L. Jiang).
[1] These authors contributed equally to this work.

https://doi.org/10.1016/j.scib.2020.06.036
2095-9273/

shown encouraging catalytic properties, very few of them can outperform the benchmark Pt-based electrocatalysts for HER [10]. Accordingly, the other approach is to minimize the required usage of noble metals by doping with the first-row transition-metal-based catalysts [11]. Ruthenium (Ru), as the cheapest Pt group metal, has also stimulated huge research interests and presented superior HER performance [12]. The Ru-based alloys, consisting of first-row transition metal and Ru elements, have been proved to be promising electrocatalysts with low cost for highly efficient HER [10]. Besides, the composites of metallic compounds and carbon materials can further improve the catalytic performance owing to the high electrical conductivity and large specific surface area of carbon materials [13].

Metal–organic frameworks (MOFs), a class of crystalline porous materials constructed by various metal nodes and organic linkers, have been demonstrated to be great precursors/templates to produce porous carbon-coated metal nanoparticles via pyrolysis [14–20]. Firstly, MOFs possess excellent chemical tunability and controlled functionalities, which allows us to regulate the types of metal elements flexibly in the node without changing the MOF structure [21,22]. Meanwhile, the carbon material produced by direct pyrolysis of organic ligand can effectively anchored the nanoparticles, ensuring their small size and high dispersion, and improving the final catalytic activity [23]. Therefore, MOFs have shown great advantages in constructing highly efficient electrocatalysts [24–26].

Herein, we report the rational design and synthesis of Ru-doped Cu nanoparticles in porous carbon (Ru-Cu@C) electrocatalysts via direct pyrolysis of the Ru-exchanged Cu-BTC MOF precursor (Fig. 1). The Ru-doped Cu electrocatalyst can serve as highly exposed active sites stabilized by the porous carbon matrix. In addition, the porous framework of MOF-derived Ru-Cu@C electrocatalyst can remarkably alleviate the diffusion barrier of electrolytes, reaction substrates and products, thus facilitating the mass transfer progress. As a result, the Ru-Cu@C composite exhibits remarkable HER activity as well as ultrahigh stability in alkaline solution, outperforming most of reported electrocatalysts so far [27,28]. Density functional theory (DFT) analysis reveals that the introduction of Ru atoms into Cu can effectively modulate surface chemistry and electronic structure, enabling a near zero hydrogen adsorption energy, which greatly benefits the final HER reaction.

2. Experimental

2.1. Synthesis of precursors RuCu-BTC

The Cu-BTC nanoparticles were synthesized according to the previously reported method with some modifications [29]. Firstly, 0.416 g of trimesic acid was dissolved in a mixed solvent of 8 mL ethanol and 24 mL *N*,*N*-dimethylformamide (DMF) to get a transparent solution. Then, 0.396 g $Cu(CH_3COO)_2{\cdot}H_2O$ dissolved in 16 mL deionized water to get a blue transparent solution, which was added into the above transparent solution. The resultant homogeneous mixture was treated with ultrasound for 1.5 h to form a blue suspension at room temperature. Afterward, the resulting blue precipitate was centrifuged, washed several times with anhydrous ethanol, and finally dried overnight at 60 °C in a vacuum oven before further use.

The as-prepared Cu-BTC nanoparticles (100 mg) were dispersed in 80 mL of the mixed solvent (the volume ratio of deionized water and anhydrous ethanol is 1:1) under stirring to get a homogeneous suspension, followed by the addition of different amounts of $RuCl_3{\cdot}xH_2O$ solution with a concentration of 10 mg mL^{-1} (Table S1 online). After stirring for 24 h at room temperature, the final products with different contents of Ru dopants, denoted as RuCu-BTC-*n* (*n* = 1, 2, 3 according to the Ru amount) were filtered and washed with anhydrous ethanol at least three times, and finally dried at 60 °C under vacuum before further use.

2.2. Synthesis of Ru-Cu@C-n (n = 1, 2, 3)

The Ru-Cu@C-1 sample was obtained by annealing the RuCu-BTC-1 precursor at 500 °C for 3 h under N_2 with a heating rate of 2 °C min^{-1}. The Ru-Cu@C-2 and Ru-Cu@C-3 samples were acquired from RuCu-BTC-2 and RuCu-BTC-3 precursors with the same way as Ru-Cu@C-1.

3. Results and discussion

3.1. Morphology and structural characterization

The Cu-BTC MOF, named as HKUST-1 was successfully synthesized by utilizing Cu^{2+} as metal source and benzene-1,3,5-tricarboxylic acid (H_3BTC) as an organic linker (Fig. 1 and Fig. S1 online). More importantly, due to the isomorphism of Cu-BTC and Ru-BTC, the dimeric Cu^{2+} units would be exchanged with other transition metal ions such as Ru^{3+}, while the basic framework of Cu-BTC MOF is still well preserved [30,31]. When Ru^{3+} is introduced, RuCu-BTC-*n* (*n* = 1, 2, 3) with different Ru contents can be obtained and present almost the same diffraction patterns as Cu-BTC [32], affirming the maintaining of intrinsic framework structure of Cu-BTC after Ru^{3+} exchange (Fig. S2a online).

The colorless supernatant was obtained by centrifuging the Ru-exchanged solution of the resultant RuCu-BTC-2, suggesting the partial replacement of Cu nodes by Ru. When the excess of $NH_3{\cdot}H_2O$ is added into the supernatant, it can be clearly found that the color of solution gradually changes from colorless to blue (Cu^{2+} + $4NH_3{\cdot}H_2O$ = $[Cu(NH_3)_4]^{2+}$ + $4H_2O$) (Fig. S3 online), which indicates the existence of Cu^{2+} in supernatant. Besides, to exclude the possibility of self-dissolution of Cu-BTC, the pure Cu-BTC nanoparticles have also been stirred in the mixed solvent of ethanol and deionized water. It is found that no color change after adding $NH_3{\cdot}H_2O$ in the supernatant. The results above confirm that the Cu nodes can be partially replaced by Ru through ion exchange (Fig. S4 online).

Scanning electron microscopy (SEM) of the as-synthesized Cu-BTC precursor clearly reveals that small nanoparticles can easily be aggregated into larger (Fig. S1 online). Then, the different amounts of Ru from $RuCl_3$ solution were introduced into the as-prepared Cu-BTC precursor through ion-exchange reaction, and the corresponding products RuCu-BTC were obtained. Compared with the original Cu-BTC, the morphology and size of products are well preserved without apparent changes (Figs. S2b and S5 online).

Subsequently, the different RuCu-BTC-*n* (*n* = 1, 2, 3) precursors were annealed under a nitrogen atmosphere at 500 °C to obtain Ru-Cu@C-*n* composites (Fig. 2a and Fig. S6 online). Taking Ru-Cu@C-2 as a representative, it is found that Ru-Cu@C-2 shows similar morphology to that of the original precursor, indicating that the pyrolysis treatment is a morphology-preserved thermal transformation process (Fig. 2a) [33]. The corresponding powder X-ray diffraction (XRD) patterns of the Ru-Cu@C-*n* (*n* = 1, 2, 3) are presented in Fig. 3a and Fig. S7 (online). A set of sharp diffraction peaks centered at 43.3°, 50.4° and 74.1°, with slight negative shifts compared with the (111), (200) and (220) planes of simulated Cu and Cu@C, can be clearly observed. This is caused by the incorperation of Ru atoms, with larger atomic radius, into the Cu lattice, bringing the expansion of the lattice constant of Cu [34]. However, there are no characteristic diffraction peaks of Ru metal

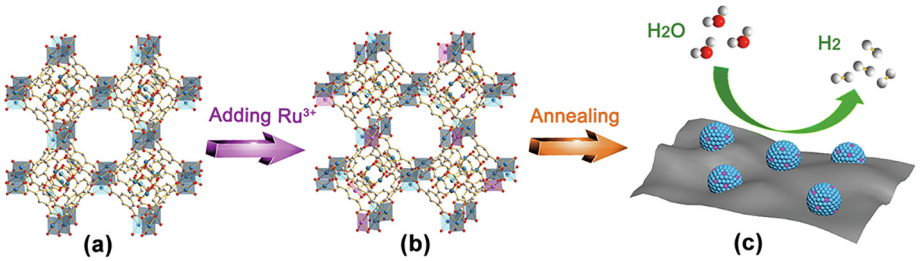

Fig. 1. (Color online) Schematic illustration of the synthesis process for the Ru-Cu@C electrocatalysts.

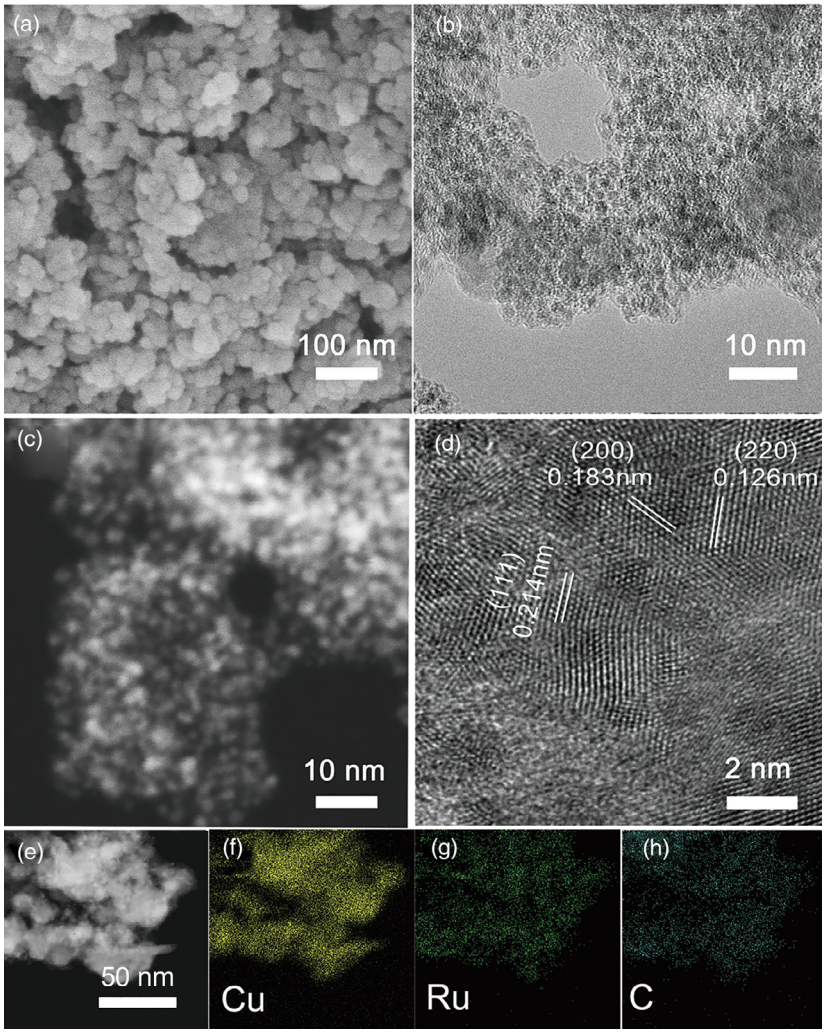

Fig. 2. (Color online) SEM and TEM images of Ru-Cu@C-2. (a) SEM, (b) TEM, (c) STEM (size histogram images), (d) HRTEM image of Ru-Cu@C-2, (e-h) HAADF-STEM images and corresponding EDX maps of Ru-Cu@C-2.

phase recognized in the powder XRD patterns, indicating that Ru atoms are successfully doped into the crystal structure of metallic Cu. Further transmission electron microscopy (TEM) and scanning transmission electron microscopy (STEM) images (Fig. 2b and c) illustrate that the isolated nanoparticles are encapsulated within carbon shells. The results suggest the carbon shells around the ultrafine nanoparticles can efficiently impede the agglomeration of these nanoparticles [35,36]. Furthermore, the atomically resolved elemental mapping images of Ru-Cu@C-2 demonstrate the homogenous dispersion of Cu and Ru elements at atomic scale (Fig. S8 online). Nitrogen sorption measurements are applied to characterize the specific surface area and the pore size distribution of the Ru-Cu@C-2 sample (Fig. 3b). Obviously, the specific surface area of Ru-Cu@C-2 is calculated to be 156 $m^2 g^{-1}$. The pore size distribution shows three strong distributions at ~27, ~40 and ~50 nm respectively, revealing the generation of abundant mesopores (inset of Fig. 3b).

The high resolution TEM (HRTEM) image of Ru-Cu@C-2 shows clear lattice fringes which are measured to be 0.214, 0.183, 0.126 nm of Ru doped Cu nanoparticles in Ru-Cu@C-2 (Fig. 2d). Meanwhile, no lattice fringes of metallic Ru are observed in the HRTEM image, indicating that Ru atoms are doped into Cu nanoparticles, in line with the XRD result (Fig. 3a). The elemental mapping images reveals that the Cu, Ru and C elements are homo-

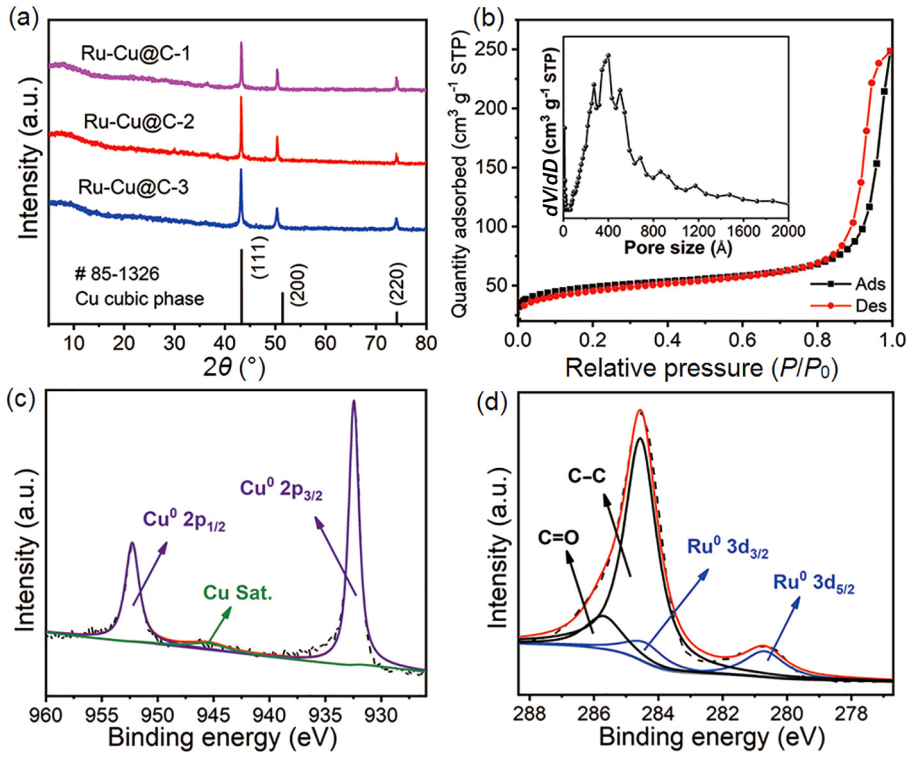

Fig. 3. (Color online) Structural and compositional analyses of Ru-Cu@C-*n*. (a) XRD patterns of Ru-Cu@C-1, Ru-Cu@C-2 and Ru-Cu@C-3. (b) N_2 adsorption–desorption isotherm of Ru-Cu@C-2 at 77 K (inset: pore size distribution). (c, d) The XPS spectrum of Ru-Cu@C-2: Cu 3p spectra and Ru 3d + C 1s spectra.

geneously distributed in Ru-Cu@C-2 (Fig. 2e–h). The Ru content is detected to be at 5.38 at% and the Ru loading of the Ru-Cu@C-2 electrode is 17.1 μg cm^{-2} based on the energy dispersive spectroscopy (EDS) results (Figs. S9 and S10 online).

Further features on the Ru-Cu@C-2 were investigated by X-ray photoelectron spectroscopy (XPS). The XPS spectra indicate the presences of Cu, Ru and C elements into Ru-Cu@C-2 (Fig. S11 online), similar to Ru-Cu@C-1 and Ru-Cu@C-3 (Figs. S12 and S13 online), with a higher Ru content than that of Ru-Cu@C-1 and lower than that of Ru-Cu@C-3 (Table S2 online). The high-resolution O 1s spectra of Ru-Cu@C-2 show the existence of H–O–H, C=O and O=O bonds, which is attributable to the trapped H_2O, CO_2 and O_2 on the surface of Ru-Cu@C-2 [37]. The Cu 2p spectra of Ru-Cu@C-2 show two sharp peaks at 932.4 and 952.3 eV, which are a little higher than those of Cu@C, mainfesting the electron transfer from Cu to Ru atoms in Ru-Cu@C-2 (Fig. 3c and Fig. S14 online) [38–41]. The high-resolution spectra of Ru 3d can be divided into two characteristic peaks with binding energies at 280.2 and 284.3 eV are attributed to metallic Ru (Ru^0 $3d_{5/2}$ and Ru^0 $3d_{3/2}$, respectively) (Fig. 3d) [42]. The high peaks located at 284.6 eV and 287.5 eV are in good agreement with C 1s due to the overlap of spectrum from C 1s (C–C and C=O, respectively) and Ru 3d, further indicating the existence of carbon around Ru-doped Cu nanoparticles.

3.2. Electrocatalytic activity characterizations

Inspired by the results above, the electrochemical HER performances for the as-prepared Ru-Cu@C-*n* catalysts were evaluated by a typical three-electrode configuration in 1 mol L^{-1} KOH. From the linear sweep voltammetry (LSV) curves, all Ru-Cu@C samples show characteristic HER catalytic behavior (Fig. 4a). It can be found that the Ru-Cu@C-1 catalyst with a low dopant content of Ru possesses an excellent HER activity with an overpotential of 78 mV. With the increase of Ru content, the Ru-Cu@C-2 catalyst exhibits a better HER activity with an overpotential of only 20 mV. Upon the further increase of Ru content, the Ru-Cu@C-3 catalyst shows an overpotential of 57 mV at 10 mA cm^{-2}, which is apparently inferior to Ru-Cu@C-2. The HER performance of Ru-Cu@C-2 is even superior to that of commercial Pt/C 20% (33 mV at 10 mA cm^{-2}) and most of previously reported Ru-based HER catalysts (Table S3 online). To clarify the kinetics of the HER process, the Tafel slope is analyzed to evaluate the rate-determining step. It can be observed that the Ru-Cu@C-2 catalyst provides an ultralow slope of 37 mV dec^{-1}, which is slightly lower than that of commercial Pt/C 20% (41 mV dec^{-1}) (Fig. 4a and b). The result indicates that the Ru-Cu@C-2 catalyst follows a typical Volmer-Heyrovsky reaction mechanism for HER [43]. Both trends of overpotential and Tafel slope are similar and exhibit the following order: Ru-Cu@C-2 < Ru-Cu@C-3 < Ru-Cu@C-1, indicating that the HER performance is closely associated with the Ru content and the Ru content in Ru-Cu@C-2 may be the closest to critical value for the best HER performance. Moreover, the pyrolysis temperature and the amount of activated carbon mixed with Ru-Cu@C-2 have also been investigated, revealing that 500 °C and 20% activated carbon used in above measurements are the most optimized conditions (Fig. S15 online).

To make a comparison, the Cu@C, with similar particle size distribution to Ru-Cu@C-2, was prepared from HKUST-1 directly (Figs. S16a and S17 online). As shown in Fig. 4c and d, the Cu@C sample shows obviously higher overpotential (363 mV at 10 mA cm^{-2}) and Tafel slope (435 mV dec^{-1}) than that of the Ru-Cu@C-2 catalyst (20 mV and 37 mV dec^{-1}). In addition, Ru@C nanocomposite were also prepared by etching the Cu of Ru-Cu@C-2. The relatively low diffreaction peaks of Ru and the absense of large metal nanoparticles in TEM image mainfest the formation of ultrafine Ru nanoclusters in Ru@C (Figs. S16b and

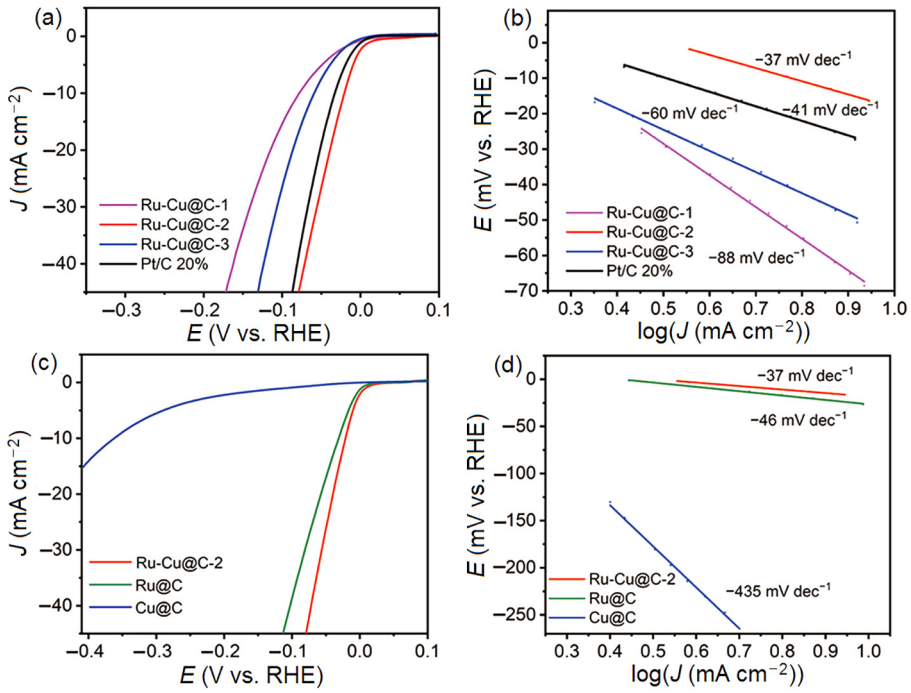

Fig. 4. (Color online) HER performance in 1 mol L^{-1} KOH solution. (a, b) HER polarization curves and the Tafel plots of Ru-Cu@C-1, Ru-Cu@C-2, Ru-Cu@C-3 and Pt/C 20% with the same mass loading. (c, d) HER polarization curves and the Tafel plots of Ru-Cu@C-2, Cu@C and Ru@C with the same mass loading. The abbreviation *E* represents potential and *J* represents current density.

S18 online). The XPS survey spectra of Ru@C verify the existance of Ru and C elements in Ru@C. However, the Cu signal is extremely low, indicating that almost all of Cu has been etched (Fig. S16c online). It can be seen that Ru@C shows a little higher surface area (276 m^2 g^{-1}) than Ru-Cu@C-2 (156 m^2 g^{-1}), with a hierarchically porous structure (Fig. S16d online). The Ru@C, with the Ru loading of 8.1 μg cm^{-2} on the electrode, demonstrates a higher overpotential of 31 mV at 10 mA cm^{-2} than that of Ru-Cu@C-2 catalyst with a higher Tafel slope (46 mV dec^{-1}), manifesting more sluggish kinetics (Table S4 online). In addition, the porous carbon obtained by etching the Cu in Cu@C also shows much lower performance (425 mV at 10 mA cm^{-2}) than Ru-Cu@C-2 (Fig. S19 online). The results above further confirm that the formation of Ru-doped Cu nanoparticles in Ru-Cu@C-2 can efficiently enhance the HER performance.

To further investigate the electron transfer kinetics of the as-synthesized catalysts during HER process, the electrochemical impedance spectroscopy (EIS) measurements were conducted. On the basis of the Nyquist plots, the obtained charge-transfer resistance (R_{ct}) values of Ru-Cu@C-1, Ru-Cu@C-2, and Ru-Cu@C-3 follow the sequence of Ru-Cu@C-1 > Ru-Cu@C-3 > Ru-Cu@C-2 (Fig. S20a online). For better comparison, the EIS measurements of Ru@C and Cu@C were also applied, illustrating that Ru-Cu@C-2 still shows the smallest R_{ct} (Fig. S21 online). In addition, the double layer capacitances (C_{dl}) of the as-synthesized catalysts were measured to evaluate the effective electrochemical active surface area (ECSA). The C_{dl} values that are strongly correlated to ECSA were collected under non-faradaic potentials through the CV curves [44]. It can be seen that the C_{dl} values follow the sequence of Ru-Cu@C-2 > Ru-Cu@C-3 > Ru-Cu@C-1 (Fig. S22 online), suggesting the highest exposure of ECSA for Ru-Cu@C-2 and this contributes effectively to its excellent HER catalytic activity. In addition to the high electrocatalytic activity, excellent stability of the catalysts is also necessary for an optimal HER performance. For the best-performed Ru-Cu@C-2 catalyst, the LSV curve after 1000 cycles of continuous CV scanning shows a negative shift of 142 mV at 50 mA cm^{-2}, which is much better than that of commercial Pt/C 20% (158 mV at 50 mA cm^{-2}) (Fig. S20b online). The TEM and XPS analyses on the tested Ru-Cu@C-2 catalyst show well maintained morphology and valance state of Cu and Ru (Figs. S23 and S24 online). Furthermore, the HER performance of Ru-Cu@C-2 stored for 6 months still exhibits an overpotential of 154 mV at 50 mA cm^{-2} with an excellent stability, similar to that of fresh Ru-Cu@C-2 catalyst (Fig. S25 online). The results above suggest the good stability of the Ru-Cu@C-2 catalyst.

3.3. Theoretical analysis

To look insight into the microscopic mechanism of HER catalytic activity on Ru-doped Cu surfaces, first-principles calculations were carried out. According to the Sabatier principle, an optimal HER electrocatalysts should possess a moderate Gibbs free energy of hydrogen adsorption (ΔG_H) to accelerate the adsorption and desorption processes. For an electrocatalyst with ideal HER catalytic activity, the value of $|\Delta G_H|$ should be zero. Therefore, we calculated the ΔG_H of different surface models including the (111), (200), (220) of cubic Ru-doped Cu phase on the basis of XRD and HRTEM analyses. Meanwhile, the corresponding surface models of pure Cu phase were also studied. In all surface models, the adsorption sites of H atoms can be classified into three types: the hollow (H) sites of Cu (111), the bridge (B) sites of Cu (200), and hollow sites of Cu (220) composed of two surface Cu atoms and one sublayer Cu atom, as depicted in Fig. 5. The computational results shown in Fig. 5a–c clearly indicate that the pure Cu surfaces are unfeasible for catalysis of HER due to the large values of $|\Delta G_H|$. Among three surface, Cu (111) features the largest value of $|\Delta G_H|$ due to the strong binding energy of H atom on it (−0.832 eV). For the Ru-doped Cu surfaces, the Ru-associated sites also exhibit strong

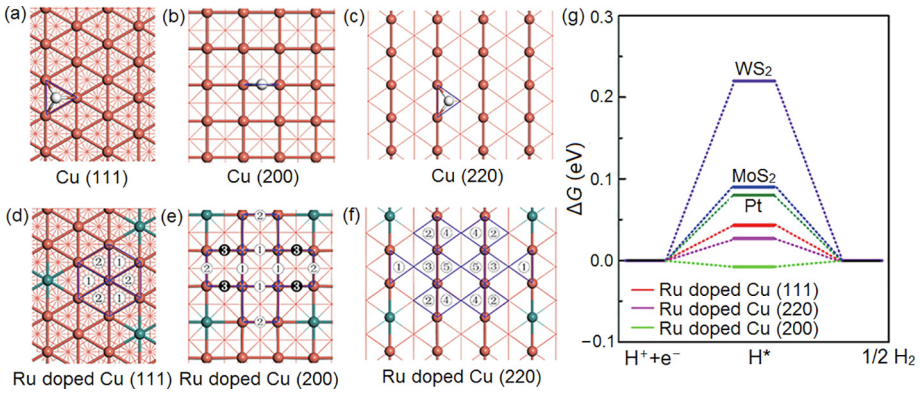

Fig. 5. (Color online) The adsorption sites of H atoms on optimized (a–c) pure and (d–f) Ru-doped surfaces. The suitable adsorption sites are marked by blue lines, and numbers. Corresponding Gibbs free energy values are listed in Table S5 (online). The numbers indicate different sites composed of Cu only as the corresponding pure surfaces, while the black "3" in (e) indicates an unstable adsorption site. The surface atoms are displayed by ball and stick model, while other atoms are displayed by line model. The orange spheres, dark green spheres and white spheres denote Cu atoms, Ru atoms and H atoms, respectively. (g) The comparison of ΔG_H values between the Ru-doped Cu surfaces and the previously reported highly active HER electrocatalysts.

binding energy for single H atom with $\Delta E(H^*)$ values smaller than −0.68 eV (Table S5 online), resulting in unfavorable ΔG_H values for HER. However, it is interesting that the dramatically reduced H binding ability could be achieved on the hollow sites far away from the substitution region. As a result, all $|\Delta G_H|$ values for H atom adsorbed on the vicinity of Cu sites are smaller than 0.1 eV (Fig. 5d–f). This finding demonstrates that the HER activity of Ru-doped Cu surfaces actually originates from the activation sites near the Cu atoms instead of those in the vicinity of Ru atoms. It is noteworthy that in Ru-doped Cu surfaces, the Ru-associated sites are more favorable to bind with H atom than the adsorption sites close to Cu atoms. However, considering the strong H-binding ability and the large amounts of Cu atoms, the H atoms would be mainly adsorbed near the Cu atoms when the Ru-associated sites are fully adsorbed by H atoms. This process could greatly facilitate the HER activity. The ΔG_H value for Hollow-4 site on Ru-Cu (220) is as small as −0.01 eV, showing the highest HER activity. The ratio of Ru-associated sites to ones near Cu atoms from small to large exhibits the following order: Cu (220) (4:14) < Cu (111) (3:6) < Cu (200) (4:6), indicating that Cu (220) has the richest active sites for HER catalysis. All $|\Delta G_H|$ values of Ru-doped Cu surfaces are smaller than other highly active HER catalysts, such as Pt (ΔG_H = 0.09 eV) and MoS_2 (ΔG_H = 0.08 eV) and WS_2 (ΔG_H = 0.22 eV) [45,46], demonstrating the highly active performance of HER on Ru-doped Cu surfaces in terms of thermodynamics. It is noteworthy that all the $|\Delta G_H|$ values of Cu-only sites on Ru-doped Cu (220) are smaller than 0.05 eV, indicating the most active facet for HER catalysis can be achieved on Ru-doped Cu (220).

To rationalize the significant reduction of $\Delta E(H^*)$ of Cu-only sites upon Ru substitution on the surface, the charge transfer of atoms within the top surface was investigated systematically. For pure Cu surfaces, all Cu atoms on surface carry small amounts of negative charges. Due to the higher electronegativity of Ru atom with respect to Cu atom, Ru atom obtains the electrons from the neighboring Cu atoms and finally an electron-accumulation region is formed around Ru substitution, as shown in Fig. S26 (online). To quantitatively assess the amount of charge transfer, we have performed the Bader charge analysis [47]. With the decrease of coordination number (CN) of Cu atom onto surface (CN = 9 for Cu (111), CN = 8 for Cu (200), CN = 7 for Cu (220)), the carried negative charges of the surface Cu atoms gradually increase from −0.030 to −0.036 |e|. With the introduction of Ru atom, almost all the surface Cu atoms lose charge, and some of them even carry a positive charge after doping the Ru atoms (Fig. S27 online). Meanwhile, the amounts of carried negative charges of Ru atom are significantly larger than those of Cu atoms. Evidently, the strong binding of H on pure Cu surfaces are mostly attributed to the considerably negative charge on the Cu atoms. Similarly, this also explains why the Ru-associated sites show the strongest binding to H atom on the Ru-doped surfaces. More importantly, the adsorption sites near the Cu atoms with the decreased negative charges on Ru-doped surfaces weaken the H binding energy and facilitate desorption of adsorbed H atom, thus lead to the close-to-zero ΔG_H values on them.

4. Conclusion

In summary, we have successfully synthesized a series of Ru-Cu@C electrocatalysts through a facile pyrolysis reaction of the as-prepared Ru-exchanged Cu-BTC under inert atmosphere. The optimized Ru-Cu@C-2 catalyst, composed of ultrafine Ru-doped Cu nanoparticles embedded into porous carbon frameworks, displays superior HER performance with an extremely low overpotential (20 mV at 10 mA cm^{-2}), ultralow Tafel slope (37 mV dec^{-1}), small charge-transfer resistance (16.8 Ω), large electrochemical active surface area and excellent stability. Both experimental results and theoretical calculations manifest that the moderate doping of Ru atoms into Cu is a key contributor to the optimal HER performance due to synergic effect between Cu and Ru atoms. The strategy presented herein holds a great promise for the rational design and synthesis of highly efficient and low-cost electrocatalysts derived from the huge diversity and tunability of MOFs.

Conflict of interest

The authors declare that they have no conflict of interest.

Acknowledgments

This work was supported by the National Key R&D Program of China (2018YFB0605700), the National Natural Science Foundation of China (51778570, 51879230, 21725101, 21871244, 21521001, and 21703145), China Postdoctoral Science Foundation (2019TQ0298, 2019M660151), and Fujian Institute of Innovation (CAS).

Author contributions

Mengya Yang and Long Jiao performed the experiments and wrote the manuscript; Huilong Dong and Liujiang Zhou preformed the DFT calculations; Changqing Teng, Dongming Yan and Tian-Nan Ye participated in part of data analysis; Xiaoxin Chen characterized HAADF-STEM image; Yi Liu and Hai-Long Jiang led the project and supervised the research. All authors discussed the results and commented on the manuscript.

Appendix A. Supplementary materials

Supplementary materials to this article can be found online at https://doi.org/10.1016/j.scib.2020.06.036.

References

[1] Li S, Ren P, Yang C, et al. Fe_5C_2 nanoparticles as low-cost HER electrocatalyst: the importance of Co substitution. Sci Bull 2018;63:1358–63.
[2] Yang Y, Fei H, Ruan G, et al. Porous cobalt-based thin film as a bifunctional catalyst for hydrogen generation and oxygen generation. Adv Mater 2015;27:3175–80.
[3] Zhang Y, Shi M, Wang C, et al. Vertically aligned $NiS_2/CoS_2/MoS_2$ nanosheet array as an efficient and low-cost electrocatalyst for hydrogen evolution reaction in alkaline media. Sci Bull 2020;65:359–66.
[4] Wang Y, Chen L, Mao Z, et al. Controlled synthesis of single cobalt atom catalysts via a facile one-pot pyrolysis for efficient oxygen reduction and hydrogen evolution reactions. Sci Bull 2019;64:1095–102.
[5] Liu Y, Liu SL, Wang Y, et al. Ru modulation effects in the synthesis of unique Rod-Like Ni@Ni_2P-Ru heterostructures and their remarkable electrocatalytic hydrogen evolution performance. J Am Chem Soc 2018;140:2731–4.
[6] Zheng Y, Jiao Y, Zhu Y, et al. High electrocatalytic hydrogen evolution activity of an anomalous ruthenium catalyst. J Am Chem Soc 2016;138:16174–81.
[7] Xia B-Y, Wu H-B, Li N, et al. One-pot synthesis of Pt-Co alloy nanowire assemblies with tunable composition and enhanced electrocatalytic properties. Angew Chem Int Ed 2015;54:3797–801.
[8] Wang J, Xu F, Jin H, et al. Non-noble metal-based carbon composites in hydrogen evolution reaction: fundamentals to applications. Adv Mater 2017;29:1605838.
[9] Zhang LZ, Jia Y, Y, Gao GP, et al. Graphene defects trap atomic Ni species for hydrogen and oxygen evolution reactions. Chem 2018;4:285–97.
[10] Li J-S, Wang Y, Liu C-H, et al. Coupled molybdenum carbide and reduced graphene oxide electrocatalysts for efficient hydrogen evolution. Nat Commun 2016;7:11204.
[11] Li F, Zhang L, Li J, et al. Synthesis of Cu-MoS_2/rGO hybrid as non-noble metal electrocatalysts for the hydrogen evolution reaction. J Power Sources 2015;292:15–22.
[12] Li W-D, Liu Y, Wu M, et al. Carbon-quantum-dots-loaded ruthenium nanoparticles as an efficient electrocatalyst for hydrogen production in alkaline media. Adv Mater 2018;30:1800676.
[13] Chen Y-Z, Wang C, Wu Z-Y, et al. From bimetallic metal–organic framework to porous carbon: high surface area and multicomponent active dopants for excellent electrocatalysis. Adv Mater 2015;27:5010–6.
[14] Zhou H-C, Kitagawa S. Metal–organic frameworks (MOFs). Chem Soc Rev 2014;43:5415–8.
[15] Lee K-J, Lee J-H, Jeoung S, et al. Transformation of metal–organic frameworks/coordination polymers into functional nanostructured materials: experimental approaches based on mechanistic insights. Acc Chem Res 2017;50:2684–92.
[16] Chen Y-Z, Zhang R, Jiao L, et al. Metal–organic framework-derived porous materials for catalysis. Coord Chem Rev 2018;362:1–23.
[17] Tang Y-J, Gao M-R, Liu C-H, et al. Porous molybdenum-based hybrid catalysts for highly efficient hydrogen evolution. Angew Chem Int Ed 2015;54:12928–32.
[18] Zhu B, Zou R, Xu Q. Metal–organic framework based catalysts for hydrogen evolution. Adv Energy Mater 2018;8:1801193.
[19] Jiao L, Wang Y, Jiang H-L, et al. Metal–organic frameworks as platforms for catalytic applications. Adv Mater 2018;30:1703663.
[20] Zhao S, Yin H, Du L, et al. Carbonized nanoscale metal-organic frameworks as high performance electrocatalyst for oxygen reduction reaction. ACS Nano 2014;8:12660–8.
[21] Kumar A, Banerjee K, Foster AS, et al. Two-dimensional band structure in honeycomb metal–organic frameworks. Nano Lett 2018;18:5596–602.
[22] Li GD, Zhao SL, Zhang Y, et al. Metal–organic frameworks encapsulating active nanoparticles as emerging composites for catalysis: recent progress and perspectives. Adv Mater 2018;30:43.
[23] Zhu B, Xia D, Zou R, et al. Metal–organic frameworks and their derivatives as bifunctional electrocatalysts. Coord Chem Rev 2018;376:430–48.
[24] Chen W-X, Pei J-J, He C-T, et al. Single tungsten atoms supported on MOF-derived N-doped carbon for robust electrochemical hydrogen evolution. Adv Mater 2018;30:1800396.
[25] Bai Q, Shen FC, Li SL, et al. Cobalt@nitrogen-doped porous carbon fiber derived from the electrospun fiber of bimetal-organic framework for highly active oxygen reduction. Small Methods 2018;2:8.
[26] Zhou TH, Du YH, Yin SM, et al. Nitrogen-doped cobalt phosphate@nanocarbon hybrids for efficient electrocatalytic oxygen reduction. Energ Environ Sci 2016;9:2563–70.
[27] Wu Y, Li G-D, Liu Y, et al. Overall water splitting catalyzed efficiently by an ultrathin nanosheet-built, hollow Ni_3S_2-based electrocatalyst. Adv Funct Mater 2016;26:4839–47.
[28] Li Y, Zhang L-A, Qin Y, et al. Crystallinity dependence of ruthenium nanocatalyst toward hydrogen evolution reaction. ACS Catal 2018;8:5714–20.
[29] Li Z-Q, Qiu L-G, Xu T, et al. Ultrasonic synthesis of the microporous metal–organic framework $Cu_3(BTC)_2$ at ambient temperature and pressure: an efficient and environmentally friendly method. Mater Lett 2009;63:78–80.
[30] Kozachuk O, Yusenko K, Noei H, et al. Solvothermal growth of a ruthenium metal–organic framework featuring HKUST-1 structure type as thin films on oxide surfaces. Chem Commun 2011;47:8509–11.
[31] Zhang W, Kozachuk O, Medishetty R, et al. Controlled SBU approaches to isoreticular metal–organic framework ruthenium-analogues of HKUST-1. Eur J Inorg Chem 2015;23:3913–20.
[32] Al-Janabi N, Hill P, Torrente-Murciano L, et al. Mapping the Cu-BTC metal–organic framework (HKUST-1) stability envelope in the presence of water vapour for CO_2 adsorption from flue gases. Chem Eng J 2015;281:669–77.
[33] Liu B, Shioyama H, Akita T, et al. Metal–organic framework as a template for porous carbon synthesis. J Am Chem Soc 2008;130:5390–1.
[34] Yao YC, Hu SL, Chen WX, et al. Engineering the electronic structure of single atom Ru sites via compressive strain boosts acidic water oxidation electrocatalysis. Nat Catal 2019;2:304–13.
[35] Ma R-G, Zhou Y, Chen Y-F, et al. Ultrafine molybdenum carbide nanoparticles composited with carbon as a highly active hydrogen-evolution electrocatalyst. Angew Chem Int Ed 2015;54:14723–7.
[36] Wei H-F, Xi Q-Y, Chen X, et al. Molybdenum carbide nanoparticles coated into the graphene wrapping N-doped porous carbon microspheres for highly efficient electrocatalytic hydrogen evolution both in acidic and alkaline media. Adv Sci 2018;5:1700733.
[37] Mahmood J, Li F, Jung SM, et al. An efficient and pH-universal ruthenium-based catalyst for the hydrogen evolution reaction. Nat Nanotechnol 2017;12:441–6.
[38] Ghodselahi T, Vesaghi MA, Shafiekhani A, et al. XPS study of the Cu@Cu_2O core-shell nanoparticles. Appl Surface Sci 2008;255:2730–4.
[39] Kusada K, Kobayashi H, Ikeda R, et al. Solid solution alloy nanoparticles of immiscible Pd and Ru elements neighboring on Rh: changeover of the thermodynamic behavior for hydrogen storage and enhanced CO-oxidizing ability. J Am Chem Soc 2014;136:1864–71.
[40] Jin Y, Chen F, Wang J, et al. Tuning electronic and composition effects in ruthenium-copper alloy nanoparticles anchored on carbon nanofibers for rechargeable Li-CO_2 batteries. Chem Eng J 2019;375:121978.
[41] Cui C-H, Li H-H, Liu X-J, et al. Surface composition and lattice ordering-controlled activity and durability of CuPt electrocatalysts for oxygen reduction reaction. ACS Catal 2012;2:916–24.
[42] Hodnik N, Jovanovic P, Pavlisic A, et al. New insights into corrosion of ruthenium and ruthenium oxide nanoparticles in acidic media. J Phys Chem C 2015;119:10140–7.
[43] Moralesguio CG, Stern LA, Hu X. Nanostructured hydrotreating catalysts for electrochemical hydrogen evolution. Chem Soc Rev 2014;43:6555–69.
[44] Wang J, Wei Z, Mao S-J, et al. Highly uniform Ru nanoparticles over N-doped carbon: pH and temperature-universal hydrogen release from water reduction. Energ Environ Sci 2018;11:800–6.
[45] Nørskov JK, Bligaard T, Logadottir A, et al. Trends in the exchange current for hydrogen evolution. J Electrochem Soc 2005;152:23–6.
[46] Hinnemann B, Moses PG, Bonde J, et al. Biomimetic hydrogen evolution: MoS_2 nanoparticles as catalyst for hydrogen evolution. J Am Chem Soc 2005;36:5308–9.
[47] Henkelman G, Arnaldsson A, Jónsson HA. Fast and robust algorithm for bader decomposition of charge density. Comput Mater Sci 2006;36:354–60.

Mengya Yang received her B.S. degree from School of Materials Science and Engineering, Central South University in 2018. She is currently a master student under the guidance of associate professor Yi Liu at Zhejiang University. Her research work is focused on the nanocomposites derived from metal–organic frameworks for electrocatalysis.

Long Jiao received his Ph.D. degree in Inorganic Chemistry from University of Science and Technology of China in 2019 under the supervision of Prof. Hai-Long Jiang. He is now a postdoc at University of Science and Technology of China in Prof. Hai-Long Jiang's group. His research work is focused on the development of metal–organic framework-based materials for electrocatalysis.

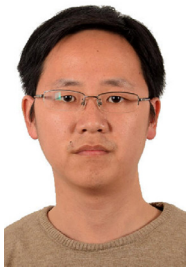

Huilong Dong received his Ph.D. degree in Material Science and Engineering from Soochow University in 2016. He is now a professor in Changshu Institute of Technology. His research area mainly locates at energy and environment related surface adsorption and catalysis with novel nanomaterials through computational approach.

Liujiang Zhou received his Ph.D. degree in 2014 from University of Chinese Academy of Sciences and performed postdoctoral research at University of Bremen, Germany (2014–2016) and at Los Alamos National Laboratory, USA (2017–2019). He started his own independent academic career as a professor at University of Electronic Science and Technology of China (2019). His research efforts are focused on optoelectronic information and energy materials, using a broad ranges of computational modeling techniques.

Yi Liu received his Ph.D. degree in 2008 from Fujian Institute of Research on the Structure of Matter, Chinese Academy of Sciences. After his postdoctoral research at Nanyang Technological University, he started his research career as an associate professor at Zhejiang University (2012). His research interest focuses on nanocomposites for energy conversion and storage.

Hai-Long Jiang received his Ph.D. degree in 2008 from Fujian Institute of Research on the Structure of Matter, Chinese Academy of Sciences and then worked at AIST (Japan) as postdoc and JSPS fellow in 2008–2011. After a postdoctoral stint at Texas A&M University (USA), he accepted a full professorship to start his independent career at University of Science and Technology of China in 2013. His main research interest is in the development of crystalline porous and nanostructured materials, crossing coordination chemistry and nanoscience, for energy-/environment-related catalysis.